ON THE EQUILIBRIUM ELECTROSTATIC POTENTIAL AND LIGHT-INDUCED CHARGE REDISTRIBUTION UNDER ILLUMINATION IN HALIDE PEROVSKITE STRUCTURES

Davide Regaldo, Aleksandra Bojar, Sean Dunfield, Pilar Lopez-Varo, Mathieu Frégnaux, Vincent Dufoulon, Shan-Ting Zhang, J Alvarez, Joseph A Berry, Jean Baptiste Puel, et al.

This is a short version of the paper submitted to the journal Progress in Photovoltaics.
It has been selected by the Executive Committee of the EU PVSEC 2021 for submission to Progress in Photovoltaics.

38th European Photovoltaic Solar Energy Conference and Exhibition

ON THE EQUILIBRIUM ELECTROSTATIC POTENTIAL AND LIGHT-INDUCED CHARGE REDISTRIBUTION IN HALIDE PEROVSKITE STRUCTURES

Davide Regaldo[a,b,c]*, Aleksandra Bojar[a,b,c], Sean P. Dunfield[d,e], Pilar Lopez-Varo[a], Mathieu Frégnaux[a,f], Vincent Dufoulon[a,g], Shan-Ting Zhang[a], José Alvarez[a,b,c], Joseph J. Berry[d], Jean-Baptiste Puel[a,h], Philip Schulz[a,g], Jean-Paul Kleider[a,b,c].

[a] IPVF, Institut Photovoltaïque d'Ile-de-France, 18, Boulevard Thomas Gobert, 91120 Palaiseau France; [b] Université Paris-Saclay, CentraleSupélec, CNRS, Laboratoire de Génie Electrique et Electronique de Paris, 91192, Gif-sur-Yvette, France; [c] Sorbonne Université, CNRS, Laboratoire de Génie Electrique et Electronique de Paris, 75252, Paris, France, [d] National Renewable Energy Laboratory, 15013 Denver West Pkwy, Golden, CO 804011;[e] Materials Science & Engineering Program, 027 UCB, University of Colorado Boulder, Boulder, CO 803032;[f] Institut Lavoisier de Versailles, Université de Versailles Saint-Quentin-en-Yvelines, Université Paris-Saclay, CNRS, UMR 8180, 45 avenue des Etats-Unis, 78035 Versailles Cedex, France7; [g] CNRS, École Polytechnique, IPVF, UMR 9006, 18, Boulevard Thomas Gobert, 91120 Palaiseau, France; [h] EDF R&D, 91120 Palaiseau, France;

Address: * davide.regaldo@ipvf.fr

ABSTRACT: Lead halide perovskites are a class of semiconductor materials which are employed as non-intentionally doped absorbers inserted between two selective carrier transport layers (SCTL), realizing a p-i-n or n-i-p heterojunction. In our study, we have developed and investigated a lateral device, based on methylammonium lead iodide ($MAPbI_3$) in which the p-i-n heterojunction develops in the horizontal direction. Our research suggests that the effective doping level in the $MAPbI_3$ film should be very low, below 10^{12} cm^{-3}. Along the vertical direction, this doping level is not enough to screen the electric field of the buried heterojunction with the SCTL. The perovskite work function is therefore affected by the work function of the SCTL underneath. From drift-diffusion simulations we show that intrinsic perovskite-SCTL structures develop mV range surface photovoltages (SPVs) under continuous illumination. However, perovskite-SCTL structures can develop SPVs of hundreds of mV, as confirmed by our measurements. We therefore analyzed the compatibility between low doping and low defect densities in the perovskite layer and such high SPV values using numerical modelling. It is shown that these high SPV values could originate from electronic processes due to large band offsets in the buried perovskite-SCTL heterojunctions, or at the SCTL - transparent conductive oxide (TCO) buried heterojunction. However, such electronic processes can hardly explain the long SPV persistence after switching off the illumination, which could be a sign that light-induced physicochemical processes are at work.

Keywords: Perovskite solar cell, surface photovoltage, drift-diffusion modelling, photoemission spectroscopy, defects.

1 INTRODUCTION

Metal halide perovskite (MHP) solar cells (PSC) have experienced a rapid increase in efficiency in the last decade. The quality of the perovskite absorber (e.g. high absorption coefficient, low recombination and high diffusion length in the domain of polycrystalline materials) and of the heterointerfaces (selectivity by carrier-blocking band offsets, low interface recombination, transparency of the selective carrier transport layers (SCTLs)) are considered as key factors for the high power-conversion efficiency (PCE) achieved [1][2].

However, despite the record improvements in PCE of PSCs, the community still faces an ongoing debate about the nature and concentration of defects in the absorber layer. Several studies report the presence of native defects in MHPs, which are dependent on the MHP deposition process [3]. Moreover, upon external stimuli, such as illumination, an oxidizing or reducing environment, or a bias voltage, defects could be created or destroyed [4][5]. Polycrystalline MHP thin films show defects both in bulk and on the grain boundaries [6]. Related to the crystal lattice properties, the perovskite's shallow defect levels have very low formation energies and could induce a nonzero doping level in the material [6][7].

Direct measurements of the doping level in perovskites, like capacitance-voltage profiling are still a major challenge. Perovskites are generally chemically reactive when brought in contact with a wide variety of metals [8]. In addition, capacitance techniques rely on the presence of a space charge region in the semiconductor, the extension of which should be modulated by the application of a voltage, a condition which is difficult to achieve for lowly doped and thin (sub-micron) semiconducting layers [9].

X-ray and ultraviolet photoemission spectroscopy (XPS, UPS) have been employed to characterize electronic and chemical properties of the perovskite material [10]. Furthermore, transient surface photovoltage (SPV) measurements in fixed capacitor configuration, Kelvin probe and Kelvin probe force microscopy (KPFM) have been employed to measure the charge extraction capabilities of perovskite - SCTL structures [11][12].

In several past studies, a combination of these techniques revealed that the Fermi level position in the bandgap of the perovskite can be changed by interfacing the MHP layer with different substrates [13][14][15][16]. However, to date the exact origin of this effect remains unresolved and could be rooted in subtle chemical interactions between the perovskite film and substrate. This supposed variability, together with the effect of different deposition techniques, produces a very complex system, loosely described by the term "p-i-n heterojunction".

In conventional, vertically stacked n-i-p or p-i-n solar

cells, the absorber is sandwiched between the SCTLs; therefore, only indirect measurements can be employed to study the impact of the SCTL on the electronic properties of the junction. In this work, we used a lateral solar cell layout (see Figure 1a), similar to the design of interdigitated back contact solar cells (IBC). The two SCTLs were deposited prior to the perovskite layer, thus forming two buried heterojunctions. In this way, the absorber properties can be measured with surface sensitive techniques and the contribution of each buried heterojunction can be separated by making the channel between the two SCTLs large enough to contain micrometric space charge regions (SCRs).

This structure was previously characterized using different techniques [17]. We focus here on the XPS, UPS, KPFM and SPV techniques and on full 3D finite-element modelling of experimental data to derive conclusions regarding the doping and defects in the perovskite material, as well as the impact of the SCTLs on the energy profiles and carrier distributions in the dark and under illumination.

2 RESULTS AND DISCUSSION

2.1 XPS surface potential analysis

We consider the perovskite lateral heterojunction device (LHJ) described in Figure 1a. It is composed of an FTO substrate on which two SCTLs, namely TiO_x and NiO_x, which act as electron transport layer (ETL) and hole transport layer (HTL), respectively, were deposited and laser scribed in order to create a channel between them ($l_{ch} > 50$ µm). Then, a $MAPbI_3$ perovskite layer was deposited on top, leaving the surface available for characterization and illumination.

We employed XPS both in scanning and imaging mode. The first method allowed us to acquire the signal rapidly, minimizing the possible radiation damage during measurement, with a total measurement time of 30 minutes. In this acquisition mode, we swept the probed area across the channel (in the x direction, as illustrated in Figure 1a) and performed local XPS measurements. We measured the variation across the channel of the $I_{3d_{5/2}}$ core level peak energy, BE_I, which is representative of the electrostatic potential variation, as shown in Figure 2. XPS scanning data show that a perceived gradual potential drop is present across the channel [17] (Figure 1b black dashed line).

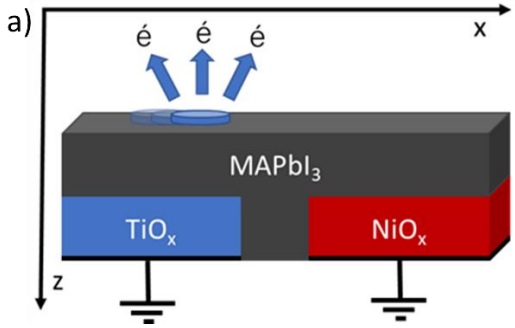

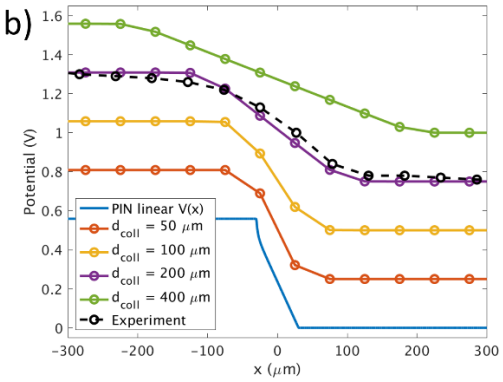

Figure 1: Sketch of the LHJ device with the representation of the XPS electron collection area in the scanning mode (a). In (b) the apparent surface electrostatic potential profile across the channel obtained from XPS experimental data (black dashed line) is compared to the one calculated from modelling using an intrinsic perovskite, under various electron collection diameters (d_{coll}). The blue solid line shows the calculated surface potential profile without convolution effect with the probe area (also corresponding to $d_{\mathrm{coll}} = 0$). The reference for the electrostatic potential (0 V) is taken on top of the NiO_x side and the origin of the x axis is taken in the middle of the channel. Curves have been shifted with respect to each other for clarity.

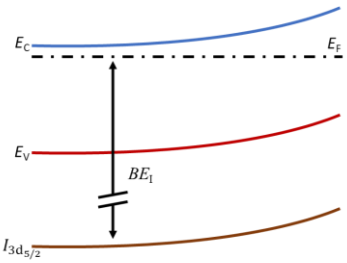

Figure 2: Sketch of the $I_{3d_{5/2}}$ core level, top of the valence band, E_V, and bottom of the conduction band, E_C, in presence of a space-dependent electrostatic potential, $q\varphi(x) = BE_I(x) = E_F - I_{3d_{\frac{5}{2}}}(x)$, q being the unit charge and E_F the Fermi level.

In this scanning XPS mode, each measured point is the average value of the collected electrons arriving from a given probe area. Therefore, to have a proper comparison with the experiments, the surface electrostatic potential values calculated from modeling have been averaged over a simulated collection distance d_{coll}, that we varied between 50 µm and 400 µm. In Figure 2b we compare the corresponding apparent surface potential profiles to the XPS experimental data (dark dashed line) and to the true calculated surface potential profile (blue curve without symbols). On the regions above the HTL and the ETL, far from the channel location, the potential is constant. The linear voltage drop in the channel is due to the perovskite being considered undoped and defect-free.

Convoluting the surface potential with the collection area of the XPS setup shows that, when the area increases, the slope of the surface potential decreases, while the perceived channel length increases. We here emphasize that a good agreement is found between the experimental data and the apparent surface potential profile calculated

with a collection diameter of 200 µm, which corresponds to the value in our experimental XPS scan mode. This good agreement was obtained assuming the perovskite to be undoped. Now, we need to study how doping and defects affect the surface potential variation and the corresponding apparent variation obtained from the XPS scan with the 200 µm collection diameter. We thus added a trap level in the bandgap close to the valence band edge. It was considered as an acceptor (E_{tA} - E_V=0.02 eV) in order to induce p-type doping [7].

We simulated the surface potential across the channel for various acceptor trap densities in the bulk perovskite and convoluted the data with the experimental electron collection area (d_{coll} = 200 µm), as shown in Figure 3. As the trap density increases, the effective p-type doping in the perovskite increases, and the potential drifts away from the linear trend, towards a parabolic-like shape. This is due to the presence of a fixed electronic charge inside the traps, which modifies the surface potential curvature. For trap density values above 10^{12} cm^{-3}, two separate SCRs appear close to the buried heterojunctions with the SCTLs along the x-direction, and a constant potential region is formed in the middle of the channel. However, this quasi-neutral region in the middle of the channel is invisible to the measurement probe due to the large electron collection distance (Figure 3).

Above 10^{15} cm^{-3} acceptor trap density in the perovskite, the electrostatic potential at the two extremities (i.e. on top of the SCTLs) starts to decouple from the respective SCTL WF, as SCRs start to form along the z-direction.

For trap density values above 10^{17} cm^{-3}, the parabolic-like shape disappears and the surface potential becomes constant along the x-direction: it does not depend anymore on the WF of the SCTL underneath.

Therefore, we conclude that acceptor trap densities higher than 10^{12} cm^{-3} are not compatible with the experimental data, as they would modify the gradual potential drop as shown in Figure 3.

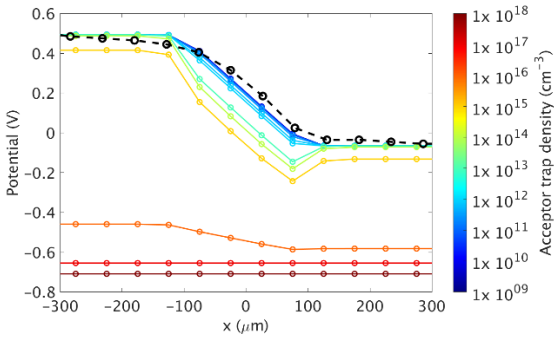

Figure 3: Surface potential of the $MAPbI_3$ perovskite across the LHJ device, convoluted with the 200 µm collection diameter of the XPS setup employed, for different shallow acceptor trap concentrations in the perovskite. The dark dashed line represents the experimental data. The surface potential $V(x)$ is referenced here to the intrinsic Fermi level $E_i(x)$: $V(x) = (E_F - E_i(x))/q$.

In Ref [19] we also considered additional high-resolution imaging mode XPS data (not shown here), that allowed us to rule out n-type doping of the perovskite with donor trap concentrations larger than 10^{12} cm^{-3}.

2.2 KPFM surface photovoltage analysis

KPFM yields the contact potential difference (CPD) between the tip of the AFM and the probed surface. Applying a DC bias between the tip and the sample or submitting the sample to illumination leads a change of CPD that depends on the charge redistribution across the layer stack. This CPD variation is therefore influenced by the presence of surface or bulk defects, or by electric fields present in surface or buried junctions and by band alignments at heterojunctions [11]. Specifically, by subtracting the CPD measured in the dark to that measured under illumination, one obtains the local surface photovoltage (SPV). Preliminary measurements on the $MAPbI_3$ perovskite LHJ device of Figure 1a were reported elsewhere [17]. We observed a large positive SPV (≈ 500 mV) on top of TiO_x, and a smaller but negative SPV on top of NiO_x (≈ -320 mV). Here we want to extend the measurements and analysis to triple cation mixed halide perovskite layers over different transport layers. We thus fabricated perovskite-SCTL structures employing a triple cation mixed halide perovskite and two different SCTLs: TiO_x and NiO_x. We characterized the bilayers with our KPFM setup, in which we illuminated the samples with a 532 nm laser centered on the KPFM tip.

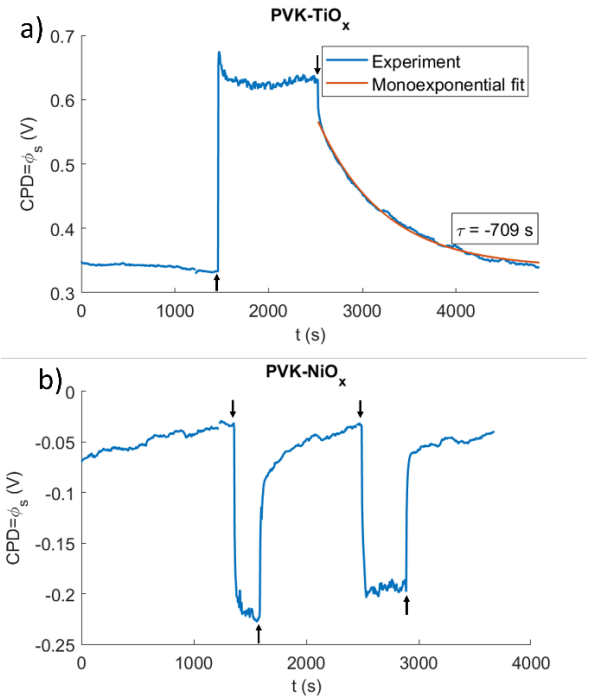

Figure 4: KPFM measurements performed on perovskite-SCTL structures, under 532 nm laser illumination. CPD measurement of (a) perovskite-TiO_x and (b) perovskite-NiO_x. Arrows indicate switch on and subsequent switch off times of the 532 nm laser illumination.

The measured sign of SPV is consistent with the nature of the SCTL underneath the perovskite, i.e. negative for the perovskite-HTL and positive for the perovskite-ETL structure (Figure 4). This is comparable to our previous measurements on $MAPbI_3$ [17]. The sign of the respective SPVs can be attributed to charge separation at the perovskite-SCTL interface. Due to the accumulation of blocked carriers inside the perovskite, a net charge builds up and the surface potential shifts under illumination [18]. The amplitude of the SPV is on the order of 300 mV for the perovskite on TiO_x, and 170 mV for the perovskite on NiO_x. Regarding the perovskite-TiO_x structure, SPVs of

150-200 mV have already been observed, while perovskite-HTL structures showed 2 orders of magnitude lower SPVs. This difference has been ascribed to a higher efficiency of charge extraction at the perovskite-ETL interface, with respect to the perovskite-HTL one [11].

The timescales of the SPV buildup after switch-on and decay after switch-off are signatures of the processes involved in the SPV formation. In our case, the rise of the SPV upon switching on the illumination is at least three orders of magnitude faster than the decay of SPV after turning off the illumination, taking into account the low temporal resolution of the instrument (~4 s).

We also observe that, for the perovskite-TiO_x sample, the photovoltage decay follows a monoexponential trend with a characteristic time constant of about 700 s. (Figure 4a).

We have employed drift-diffusion modelling to unveil the root causes of the SPV and study its dynamics under continuous monochromatic illumination in our perovskite - SCTL bilayers. For comparison with experimental data, we have chosen the same light intensity employed in the KPFM measurements (~8 W/cm^2).

We start with the ideal case, in which the perovskite is intrinsic and without defect states in the bandgap, as suggested by the electrostatic potential measurements in Sec. 2.1, and the SCTL is also without defect states in the bandgap but doped ($N_{\mathrm{dop}} = 10^{17}\mathrm{cm}^{-3}$). In addition, we consider zero band offset between the perovskite and the SCTL for the type of carriers that should be extracted at this interface. At equilibrium, the perovskite being undoped and defect-free, the position of the Fermi level in the perovskite is imposed by the doped SCTL underneath, and only a low built-in voltage of about 100 mV forms across the heterojunction.

Under illumination, electrons and holes are separated at the heterointerface: holes accumulate in the perovskite, while electrons accumulate inside the ETL. The sign of the calculated SPV is therefore positive. The charge redistribution is opposite in the perovskite - HTL structure, where the sign is negative. Noticeably, the amplitude of the SPV in both types of structures is lower than 1 mV (Figure 5).

In conclusion, this simple modelling of the perovskite-ETL and perovskite-HTL structures cannot explain the large amplitudes that are experimentally observed. In addition, the calculated transients are much faster, with stabilization times lower than 1 µs. We therefore studied which other factors could affect rise, decay time and magnitude of the SPV.

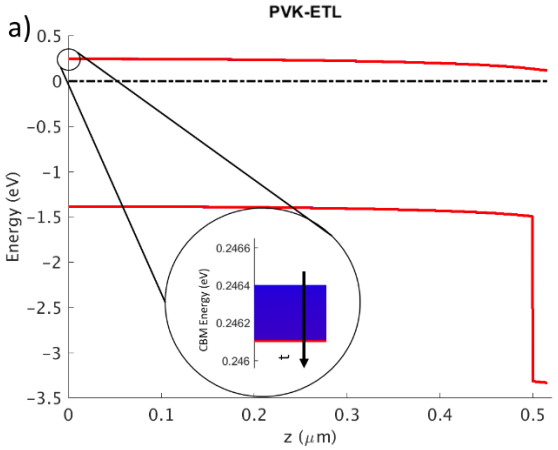

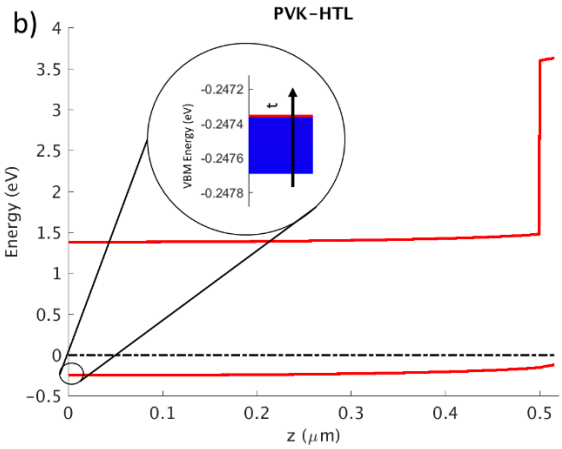

Figure 5: perovskite (PVK)-SCTL band diagrams under illumination; (a) PVK-ETL, and (b) PVK-HTL; the small time-dependent shift of the surface potential after switch-on is magnified in the insets (positive for PVK-ETL, negative for PVK-HTL). The black arrows indicate the direction of the shift of the surface potential as a function of time.

A built-in voltage across a buried (hetero)junction is usually considered as a primary source of surface photovoltage formation. Regarding the perovskite - TiO_x structure, the presence of effective p-type doping in the perovskite would determine a built-in voltage across the heterojunction, since TiO_x has been considered as n-type (with a donor concentration $N_{\mathrm{d}} = 10^{17}\mathrm{cm}^{-3}$). Thus, although the XPS mapping results presented in Sec. 2.1. suggest that high doping of the perovskite is unlikely, we calculated the SPV response under experimental illumination conditions for different doping density values of the perovskite. Results of the transient SPV curves for both switch-on and switch-off are displayed in Figure 6, showing that the magnitude of the SPV and corresponding decay times do indeed increase with the perovskite acceptor doping concentration.

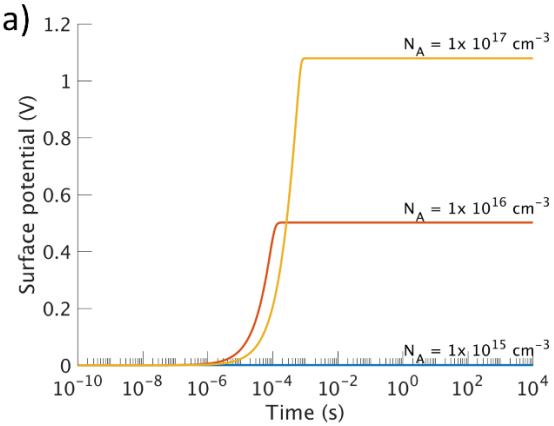

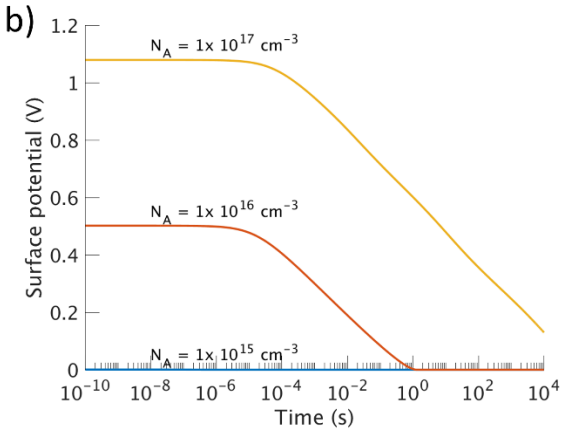

Figure 6: Perovskite - TiO_x transient SPV simulations for different values of acceptor dopant concentration in the perovskite; (a) build-up of SPV after illumination is switched on, and (b) SPV decay after illumination is switched off.

However, the characteristic decay time of the simulated SPV is considerably lower than the 700 s observed experimentally. We also note that the simulated transient after switch-off exhibits a non-exponential decay, in contrast with the exponential behavior observed experimentally for long times (Figure 4a). Therefore, p-type doping of the perovskite would be unable to explain the experimental SPV results, which further confirms the results from XPS data analysis in Sec. 2.1.

For selectivity purposes, large valence band offset at the ETL interface is preferable in order to prevent holes, generated in the perovskite, from diffusing into the ETL. At the same time the conduction band offset should be small in order to facilitate electron collection. Thus, the conduction band offset defined as the difference at the interface between the bottom of the conduction band in the perovskite, $E_{C,pvk}$, and that in the TiO_x, E_{C,TiO_x}, $\Delta E_C = E_{C,pvk} - E_{C,TiO_x}$, should ideally be close to zero. However, we found that a significantly positive value could be a source of large surface photovoltage, as depicted in Figure 7.

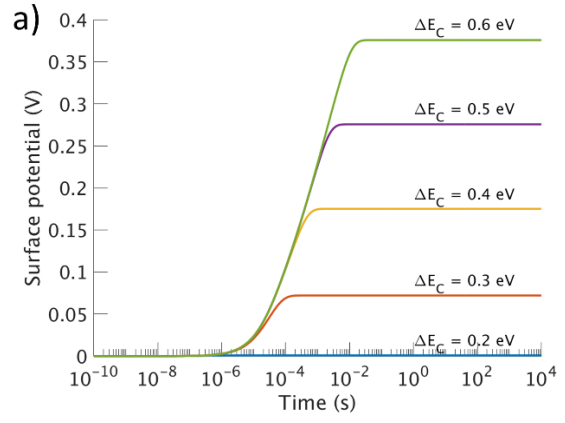

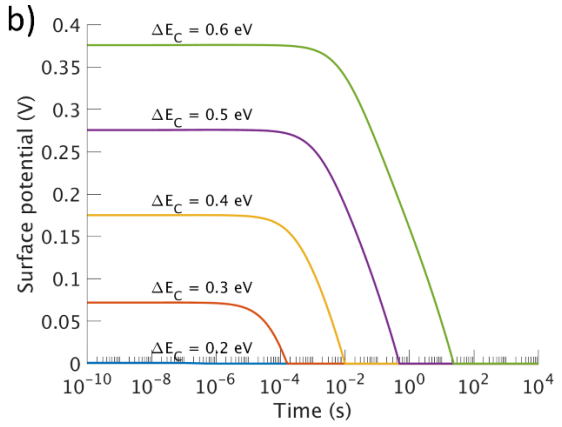

Figure 7: Perovskite - TiO_x transient SPV simulations for different values of conduction band offset, $\Delta E_C = E_{C,pvk} - E_{C,TiO_x}$; (a) build-up of SPV after illumination is switched on, and (b) SPV decay after illumination is switched off.

Under illumination, electron-hole pairs are continuously generated inside the perovskite layer. In steady state conditions, however, the net flux of electrons across the perovskite - ETL heterojunction should be zero (open circuit conditions). For positive values of the conduction band offset, the electrons reinjected towards the perovskite from the TiO_x have to overcome a potential barrier in a thermionic emission process. If the barrier height increases, the amount of electrons accumulated in the TiO_x layer has to increase, in order to keep a net zero flux of electrons in steady state, thus increasing the negative charge in TiO_x. An opposite positive charge of holes forms in the perovskite, which shifts the surface potential towards more positive values. This shift is represented in Figure 8a, where the transition from blue to red curves shows the accumulation of holes in the perovskite as a function of time, after illumination is switched on. The carrier separation is also highlighted in Figure 8b: increasing the conduction band offset value leads to larger accumulation of holes in the perovskite, and of electrons in the TiO_x layer.

The same reasoning would be valid for a perovskite - HTL structure with opposite values of the valence band offset with respect to the ones shown in Figure 7.

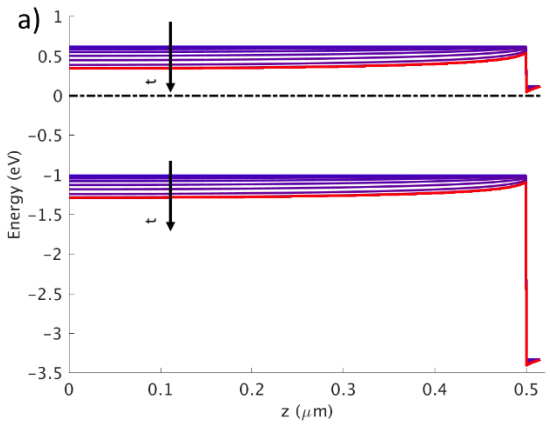

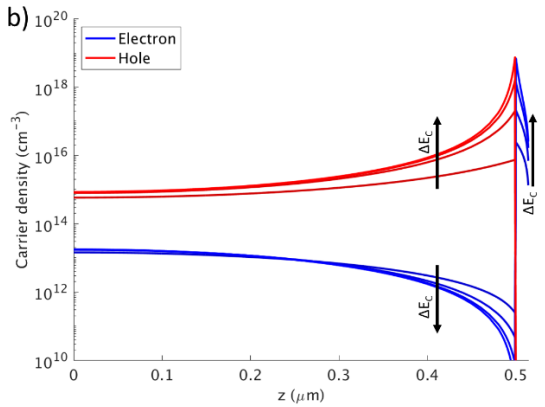

Figure 8: Band diagram evolution after illumination is switched on for perovskite - TiO_x (a), and (b) photogenerated carrier distribution across the same heterostructure under illumination in steady state, for different values of conduction band offset. The interface between perovskite and TiO_x is located at $z = 0.5$ µm .

Conduction band offsets of 0.5 and 0.6 eV provide SPVs of 0.28 and 0.38 V, respectively, which are comparable to the experimental values. However, the characteristic decay time of the SPV related to this process is again considerably lower than experimentally observed, and the simulated transient at switch-off is non-exponential. In addition, we expect that such large values of conduction band offset would limit the efficiency of solar cells. In conclusion, the experimental SPV amplitude and transients cannot be explained solely by the conduction band offset at the perovskite-SCTL heterojunction.

In addition to doping and band offset considerations, we studied how the SPV is affected by the presence of defects in the SCTL and how it could depend on the WF of the contact electrode. Indeed, defects could trap photogenerated carriers selectively injected in the SCTL, generating an SCTL-dependent SPV, while changing the WF of the contact electrode can introduce a Schottky contact at the back of TiO_x, which also affects the SPV.

The full analysis, described in [19], shows that a conduction band offset of 500 meV may explain the amplitude of the SPV but is unable to describe the transient behaviour, while the decay time after switch-off is more compatible with the presence of a modest ($\simeq$ 400 meV) difference between the back contact and the TiOx work functions, which however cannot reproduce the measured SPV amplitude.

3 DISCUSSION AND CONCLUSIONS

In this study, we combined experiments and modelling on specific perovskite-SCTL structures to discuss the equilibrium electrostatic potential distribution and the redistribution of charges upon illumination. On the one hand, our analysis conducted in equilibrium conditions supports the hypothesis of a low effective doping density, smaller than 10^{12} cm^{-3}, inside the perovskite. On the other hand, from drift-diffusion simulations for the bilayers under study, we showed that nearly intrinsic perovskite - moderately doped SCTL structures provide surface photovoltage values lower than 1 mV, while experimental values exceed hundreds of mV under the same continuous illumination conditions. Regarding the perovskite - TiO_x structure, we also excluded the effect of band offsets at the buried heterojunction due to decay time after switching off the illumination. Considering the presence of a contact electrode at the bottom of the structure, we studied the influence of its work function, which affects the SPV. Also in this case, however, varying uniquely this parameter does not allow to fit both the SPV magnitude and decay times.

We can suggest that the large timescale of the photovoltage decays of the perovskite-ETL samples could indicate the occurrence of reversible chemical reactions at the perovskite/SCTL interface, which were not considered in drift-diffusion simulations. Those reactions could be driven by the presence of a net charge inside the perovskite under illumination, due to the presence of the SCTLs and the TCO.

4 REFERENCES

[1] N. G. Park, Mater. Today 18 (2015) 65.
[2] M. I. H. Ansari, A. Qurashi, M. K. Nazeeruddin, J. Photochem. Photobiol. C Photochem. Rev. 35 (2018) 1.
[3] W. J. Yin, T. Shi, Y. Yan, Appl. Phys. Lett. 104 (2014).
[4] D. Meggiolaro *et al.*, Energy Environ. Sci. 11 (2018) 702.
[5] S. G. Motti *et al.*, Adv. Mater. 31 (2019) 1.
[6] H. Jin *et al.*, Mater. Horizons 7 (2020) 397.
[7] J. Euvrard, Y. Yan, D. B. Mitzi, Nat. Rev. Mater. 6 (2021) 531.
[8] L. Zhao *et al.*, ACS Energy Lett. 1 (2016) 595.
[9] O. Almora, C. Aranda, E. Mas-Marzá, G. Garcia-Belmonte, Appl. Phys. Lett. 109 (2016).
[10] S. Béchu, M. Ralaiarisoa, A. Etcheberry, P. Schulz, Adv. Energy Mater. 10 (2020) 1.
[11] B. N. Lee, S. Kirmayer, E. Edri, G. Hodes, D. Cahen, J. Phys. Chem. Lett. 5 (2014) 2408.
[12] J. R. Harwell *et al.*, Phys. Chem. Chem. Phys. 18 (2016) 19738.
[13] T. Gallet, D. Grabowski, T. Kirchartz, A. Redinger, Nanoscale 11 (2019) 16828.
[14] P. Schulz, L. L. Whittaker-Brooks, B. A. Macleod, D. C. Olson, Y. L. Loo, A. Kahn, Adv. Mater. Interfaces 2 (2015).
[15] E. M. Miller *et al.*, Phys. Chem. Chem. Phys. 16 (2014) 22122.
[16] A. Zohar, M. Kulbak, I. Levine, G. Hodes, A. Kahn, D. Cahen, ACS Energy Lett. 4 (2019) 1.
[17] S. P. Dunfield *et al.*, (2021).
[18] L. Qiu, S. He, L. K. Ono, Y. Qi, Adv. Energy Mater. 10 (2020) 1.
[19] D. Regaldo *et al.*, this conference, submitted to Progress in Photovoltaics.